cosmetics

MDPI

Article

Safflower Seed Oil and Fermented *Artemisia annua* Oil Restore UVB-Induced Skin Barrier Dysfunction by Attenuating Inflammation and Promoting Extracellular Matrix Remodeling

Jinjin Liu [1,†], Qian Wang [2,†], Jialin Zhong [1], Xiaoqing Wang [1], Mei Zhang [1], Yushu Wang [1], Ya Zhao [2], Le Zhu [2], Runshuang Lu [2,*], Haidong Jia [2,*] and Gang Ma [1,*]

[1] Key Laboratory for the Genetics of Developmental and Neuropsychiatric Disorders (Ministry of Education), Bio-X Institutes, Shanghai Jiao Tong University, Shanghai 200240, China
[2] Shanghai Jahwa United Co., Ltd., Shanghai 200233, China
* Correspondence: lurunshuang@jahwa.com.cn (R.L.); jiahaidong@jahwa.com.cn (H.J.); magang@sjtu.edu.cn (G.M.); Tel.: +86-21-34207232 (G.M.)
† These authors contributed equally to this work.

Abstract

Background: As the body's first line of defense against environmental stressors, the skin is highly susceptible to UVB-induced damage, which triggers inflammation and impairs barrier function. This study investigates the protective effects of safflower seed oil (SSO) and fermented *Artemisia annua* oil (FAAO) against UVB-induced skin injury. Methods: The protective effects of SSO and FAO against UVB irradiation was first tested in HaCaT keratinocyte. Subsequently, a UVB-irradiated SKH-1 mouse model was established to evaluate these two oils. RNA-seq analysis was employed to investigate the potential molecular mechanisms by which SSO and FAO repair the skin barrier. Results: In vitro experiments demonstrated that SSO (0.25%) and FAAO (0.1%) significantly enhanced HaCaT keratinocyte viability following UVB exposure while selectively modulating pro-inflammatory cytokine production. In a UVB-irradiated SKH-1 mouse model, standalone SSO or FAAO treatment partially ameliorated epidermal hyperplasia and restored UV-reduced collagen content, while the 1:1 SSO/FAAO combination exhibited superior efficacy in restoring skin architecture, reducing erythema and edema, and suppressing immune cell infiltration. Transcriptomic profiling revealed that the combined treatment promoted structural repair by attenuating inflammatory responses and preserving extracellular matrix homeostasis. Conclusions: Together, these findings underscore the potential of SSO/FAAO as a multifunctional botanical intervention for mitigating UVB-induced cutaneous damage.

Keywords: safflower seed oil; fermented *Artemisia annua* oil; UVB; inflammation; extracellular matrix

Academic Editor: Bryan Fuller

Received: 2 February 2026
Revised: 4 March 2026
Accepted: 10 March 2026
Published: 20 March 2026

1. Introduction

As the largest organ and the primary defense barrier against external environmental challenges, the skin plays an irreplaceable role in maintaining systemic homeostasis through its intricate structure and multifunctional properties [1]. The histological architecture of the skin follows a three-level hierarchical pattern of epidermis-dermis-subcutaneous tissue, with each level possessing unique biological properties and physiological roles [2]. The epidermis, dominated by keratinocytes, undergoes a terminal differentiation process involving basal layer proliferation, spinous layer differentiation, granular layer maturation, and stratum corneum desquamation. This process is tightly regulated by the Notch

signaling pathway and Wnt/β-catenin pathway, ensuring epidermal homeostasis [3]. The dermis maintains mechanical strength via collagen and elastin secreted by fibroblasts while participating in inflammatory signaling [4]. Recent studies highlight that the skin is not merely a physical barrier but also an immunologically active organ, with Langerhans cells in the epidermis and dermal dendritic cells forming a sophisticated immune surveillance network [5]. This structural complexity enables the skin to serve as the first line of defense against environmental insults, such as ultraviolet (UV) radiation and pathogens.

Midwave ultraviolet radiation (UVB, 290–320 nm) penetrates the epidermal basal layer and damages the superficial dermis. Its phototoxic effects manifest as abnormal epidermal thickening, desquamation of the stratum corneum, and persistent erythema due to dermal vasodilation, leading to skin roughness and photoaging [6]. Histopathological studies demonstrate that UVB exposure increases murine epidermal thickness by 1.8-fold within 24 h, and significantly disrupts stratum corneum integrity [7].

UVB triggers cascading inflammatory responses through direct DNA damage and activation of oxidative stress pathways. Photon energy absorbed by epidermal DNA induces cyclobutane pyrimidine dimer (CPD) formation, activating the ATM/ATR-Chk1 signaling axis to drive p53-dependent apoptosis and release damage-associated molecular patterns (DAMPs) [8]. Concurrently, UVB stimulates NADPH oxidase (NOX) and disrupts mitochondrial electron transport chains, causing reactive oxygen species (ROS) overproduction. This oxidative surge phosphorylates nuclear factor-κB (NF-κB) and activator protein-1 (AP-1), initiating pro-inflammatory cytokine transcription, leading to excessive expression of interleukin-1β (IL-1β), IL-6, and tumor necrosis factor-α (TNF-α). Clinical studies reveal that a 2× minimal erythema dose (MED) of UVB elevates epidermal IL-1β mRNA by 4.3-fold within 6 h, correlating with erythema severity [9]. TNF-α exacerbates photoaging by activating matrix metalloproteinases (MMP-1/MMP-3), which degrade type I collagen in the dermis, forming characteristic pathological features of photoaging [10].

Within 6–12 h post-irradiation, the skin undergoes immune microenvironment remodeling marked by $CD45^+$ leukocyte infiltration. These infiltrating cells—including $CD11b^+Ly6C^+$ monocytes, $Ly6G^+$ neutrophils, and $CD3^+$ T cells—migrate into the dermis, disrupting extracellular matrix homeostasis through elastase and MMP secretion [11]. UV-generated DAMPs bind to Toll-like receptors (TLRs) on macrophages, triggering MyD88-dependent NF-κB nuclear translocation and the explosive release of IL-6 [12,13] and IL-1β [14]. This process establishes a self-perpetuating "inflammation-matrix degradation-reinflammation" positive feedback loop. Enhanced vascular permeability and sustained immune cell recruitment, coupled with MMP-mediated collagen network destruction, culminate in clinical manifestations of photodamage, including erythema, edema, and wrinkle formation [15].

Although current anti-inflammatory and photoprotective strategies exist, conventional synthetic drugs often pose risks of skin irritation or drug resistance. Consequently, developing natural, safe, and efficacious plant-derived ingredients has gained momentum. Recent investigations into plant-derived oils for mitigating UVB-induced skin damage highlight their anti-inflammatory and antioxidant properties. Evening primrose oil (*Oenothera biennis*), rich in γ-linolenic acid (GLA), suppresses NLRP3 inflammasome activation, significantly reducing IL-1β maturation and release in murine models. However, its effects on IL-6 and TNF-α remain unclear, and long-term use may increase lipid peroxidation due to oxidation of highly unsaturated fatty acids [16]. Sea buckthorn oil (*Hippophae rhamnoides*), containing palmitoleic acid, antagonizes the JAK-STAT pathway, reducing IL-6 expression by 39% in HaCaT cells. Nevertheless, clinical studies indicate its carotenoid components may induce photosensitivity under UV exposure, limiting applicability. Argan oil (*Argania spinosa*) polyphenols inhibit the ROS-dependent TNF-α/NF-κB pathway via iron chelation,

decreasing TNF-α mRNA expression by 62% in vitro. However, its high oleic acid content reduces transdermal efficiency due to hydrophobicity [17]. While these studies reveal the potential of plant oils in modulating individual inflammatory factors, their multicomponent synergies and capacity to regulate multiple cytokines remain underexplored.

Safflower seed oil (SSO) and fermented *Artemisia annua* oil (FAAO) are gaining interest for their distinct bioactive properties: SSO is rich in linoleic acid, while FAAO contains artemisinin derivatives enhanced through fermentation. Despite their potential in mitigating UVB-induced skin damage, systematic studies into their individual and combined effects remain lacking. This gap hinders the development of natural formulations that synergistically address UVB-triggered inflammation and barrier dysfunction.

This study investigates the therapeutic potential of SSO and FAAO, administered individually and in combination, in mitigating UVB-induced skin damage by modulating inflammatory pathways and promoting epidermal repair mechanisms. The findings provide a foundation for developing novel botanical-based photoprotective formulations with integrated anti-inflammatory and barrier-restoring capacities.

2. Materials and Methods

2.1. Cell Culture

The HaCaT cells, developed from normal adult skin keratinocytes [18], were kindly provided by Prof. Yuping Lai, East China Normal University, Shanghai, China. Cells were maintained in DMEM medium supplemented with 10% fetal bovine serum (FBS) and 1% penicillin-streptomycin dual antibiotics and cultured at 37 °C in a humidified incubator with 5% CO_2.

2.2. Crystal Violet Staining

HaCaT cells were cultured in 24-well plates until the density reached approximately 70% and then washed once with PBS. The cells were then irradiated with different UVB dosages, and fresh medium was added after irradiation. After 24 h, 4% PFA was added to fix the cells (room temperature, 15–20 min), which were then washed twice with PBS. Crystal violet solution was then added to stain the cells (room temperature (RT), protected from light, 10–30 min). The cells were then gently washed with ddH_2O and left to dry. Images were acquired with a camera and quantitative analysis was performed using Image J software (v1.54g).

2.3. CCK-8 Cytotoxicity Assay

HaCaT cells were cultured in a 96-well plate to a density of about 70%, and the medium with different concentrations of DMSO/SSO/FAAO was added for 24 h (SSO and FAAO formulations were provided by Northstar Lipids Ltd. (Lincolnshire, UK) and Hangzhou SHIGUANGXINYA Biotech Co., Ltd. (Hangzhou, China), respectively. To determine the optimal concentrations of SSO and FAAO, HaCaT cells were cultured for 16 h, washed with PBS, and exposed to UVB irradiation (500 J/m^2). Subsequently, cells were treated with varying concentrations of SSO or FAAO for 24 h. Cell viability was evaluated using the CCK-8 assay kit (Life-iLab, Shanghai, China, AC11L054) according to the manufacturer's instructions. Absorbance was measured at 450 nm using a microplate reader, and cell viability was calculated using the following formula: cell viability (%) = (OD (control) − OD (blank))/(OD (test) − OD (blank)) × 100.

2.4. Animal Procedures

All experimental procedures were conducted in compliance with the ARRIVE guidelines and approved by the Institutional Animal Care and Use Committee (IACUC) of

Shanghai Jiao Tong University, with strict adherence to the 3Rs principles (Replacement, Reduction, Refinement). Male SKH-1 hairless mice (aged 7–8 weeks, body weight: ~25 g) were purchased from Shanghai SLAC Laboratory Animal Co., Ltd. (Shanghai, China). Standard housing conditions comprised: (1) group size $\leq$ 5 animals/cage, (2) autoclaved chow and filtered water available ad libitum, and (3) controlled 12 h light/dark cycles. Environmental enrichment and sterile bedding renewal were performed every 48 h. Seven-week-old SKH-1 hairless mice were randomized into five groups (n = 3): Untreated control (CON); UVB irradiation (UVB); UVB + 100 µL topical SSO (UVB + SSO); UVB + 100 µL topical FAAO (UVB + FAAO); and UVB + SSO:FAAO (1:1, v/v) compound (UVB+ Compound). UVB irradiation (2000 J/m^2) was administered every 48 h for 7 days using a Scientz03-II UV crosslinker (Ningbo Scientz Biotechnology Co., Ltd., Ningbo, China). Test formulations were applied topically 30 min prior to irradiation. Clinical evaluations including erythema, scaling, and sunburn reactions were systematically documented through standardized dorsal photography at 48 h intervals. Transepidermal water loss (TEWL) was measured using a GPSkin Barrier® device (GPOWER, Seoul, Republic of Korea).

2.5. Hematoxylin and Eosin Staining

Tissue specimens were fixed in 4% PFA for 24 h, processed through graded ethanol and xylene, and paraffin embedded. Sections (6 µm) were deparaffinized, rehydrated, and stained using the Hematoxylin and Eosin (H&E) Staining Kit (Beyotime Biotech Inc., Shanghai, China, C0105S) according to the manufacturer's protocol. Nuclei were stained with hematoxylin (5 min), differentiated, and counterstained with eosin Y (20 s). After dehydration and xylene clearance, slides were coverslipped with neutral resin and imaged via bright-field microscopy.

2.6. Masson's Trichrome

Tissue specimens were fixed in 4% paraformaldehyde (PFA) for 24 h, dehydrated through a graded ethanol series, cleared in xylene, and embedded in paraffin. Sections of 6 µm thickness were cut, deparaffinized, rehydrated, and stained using the Beyotime Masson's Trichrome Staining Kit (Beyotime Biotech Inc., Shanghai, China, C0189S) following the manufacturer's instructions. After staining, slides were mounted with neutral resin and visualized under bright-field microscopy. (Nuclei appear purple due to hematoxylin staining; cytoplasm is stained red by ponceau-acid fuchsin; collagen fibers are colored green by light green.)

2.7. Immunofluorescence Staining

Skin tissues underwent 4% PFA fixation (24 h), 30% sucrose cryoprotection (4 °C/overnight), and were cryosectioned at 6 µm. Sections were blocked with 10% FBS/PBS for 1 h at RT, followed by primary antibody incubation (4 °C/16–18 h) and Alexa Fluor-conjugated secondary antibody labeling (1:800, light-protected/2 h/RT). After PBS washes, slides were mounted with DAPI-containing ProLong™ Gold Antifade reagent (Thermo Fisher Scientific, Waltham, MA, USA), sealed, and imaged using a Leica SP8 confocal system (4 °C storage). The following antibodies were used for immunostaining: Rabbit anti-F4/80 (Cell Signaling Technology, Danvers, MA, USA, #70076); Rat anti-CD45 (BioLegend, San Diego, CA, USA, #202211); Donkey anti-Rabbit IgG (H + L) Alexa Fluor™ Plus 488 (Thermo Fisher Scientific, Waltham, MA, USA, A32790); Donkey anti-Rat IgG (H + L) Alexa Fluor™ Plus 488 (Thermo Fisher Scientific, Waltham, MA, USA, A-21208).

2.8. RNA Isolation and RT-PCR

The total RNA of murine dorsal skin tissues and cultured cells was extracted by using TRIzol® Reagent (Vazyme, Nanjing, China, R401-01) following the manufacturer's

standardized workflow under RNase decontamination conditions. RNA (up to 1 µg) was used to synthesize cDNA using the HiScript III 1st Strand cDNA Synthesis Kit (Vazyme Biotech Co., Ltd., Nanjing, China, R312-01). Then, qRT-PCR was performed with the SYBR Green Mix (Vazyme Biotech Co., Ltd., Nanjing, China, Q311-02). The housekeeping gene 18s was used to normalize gene expression in samples. The primers used for RT-PCR are shown in the Supplementary Table S1.

2.9. GC-MS Analysis

The GC-MS (gas chromatography-mass spectrometry) analysis, including the compositional testing and characterization of SSO and FAAO, was performed by Shanghai Weipu Testing Technology Co., Ltd., Shanghai, China.

2.10. RNA Sequencing

RNA sequencing was performed on day 7 using dorsal skin samples from mice allocated to three experimental groups: Untreated control (CON), UVB irradiation (UVB), and UVB + SSO:FAAO (1:1, v/v) compound (UVB + Compound). RNA sequencing was conducted by BGI Genomics Co., Ltd. (Shenzhen, China). Subsequent bioinformatics analyses were performed using the Dr. Tom platform (https://biosys.bgi.com), including principal component analysis (PCA), volcano plots of differentially expressed genes (DEGs), Kyoto Encyclopedia of Genes and Genomes (KEGG) pathway enrichment analysis, and heatmap visualization. Differentially expressed genes (DEGs) were identified using the DEGseq2 method with screening thresholds of q-value ≤ 0.05 and $|\log2(\text{fold change, FC})| \geq 1$.

2.11. Statistical Analysis

All experiments were performed at least in triplicate. When applicable, data were expressed as mean ± SEM. Statistical analyses were conducted using GraphPad Prism version 10 (GraphPad Software, San Diego, CA, USA). For comparisons between two groups, Student's two-tailed t-test was used. For multiple group comparisons, one-way or two-way analysis of variance (ANOVA) was performed, followed by Tukey's multiple comparisons test or the Brown–Forsythe test as appropriate. Statistical significance was defined as * $p < 0.05$, ** $p < 0.01$, *** $p < 0.001$, and **** $p < 0.0001$; 'ns' indicated no statistically significant results.

3. Results

3.1. Component Characterization of SSO and FAAO

Safflower seed oil (SSO), a plant oil extracted from *Carthamus tinctorius* L. seeds, was characterized using GC-MS, revealing 42 characteristic compounds. The chemical composition predominantly comprised lipids, aliphatic aldehydes, and oxygenated terpenoids.

The lipid profile was dominated by 2-linoleoylglycerol (57.10%), followed by trilinolein (19.54%) and ethyl linoleate (5.33%), with additional structural diversity from free fatty acids (linoleic acid, 5.28%) and glycidyl palmitate (4.11%). Aldehydes included trans-2,4-decadienal (0.99%) and 2,4-decadienal (0.70%), while betulin (1.69%) represented the sole terpenoid. Trace components such as 1,2-dipalmitin (0.56%) and glycerol monooleate (0.37%) further enriched the lipid complexity, establishing SSO as a glycerol ester-rich system with structural heterogeneity and functional potential (Supplementary Figure S1 and Table S2).

Fatty acid profiling revealed a predominance of unsaturated species, with linoleic acid (C18:2n6c, 69.1%) and oleic acid (C18:1n9c, 18.7%) constituting 88.7% of total fatty acids, alongside minor α-linolenic acid (Supplementary Table S3).

The GC-MS total ion chromatogram of FAAO (Supplementary Figure S2) revealed 54 compounds. Mass content analysis demonstrated that fatty acid glycerides dominated

the composition (93.4–99.4%), with trace components including squalene (0.01–0.02%), vitamin E (0.02–0.04%), and γ-sitosterol (0.08–0.14%). Relative mass percentage analysis identified three aldehydes: 2-heptenal, trans-2-decenal, and the predominant trans-2,4-decadienal (7.38%). Six terpenoids were detected, notably β-caryophyllene (8.97%), B-selinene, and caryophyllenol. The sterol system comprised three components: γ-sitosterol (6.52%), campesterol (10.11%), and stigmasterol (5.36%). Vitamin E (3.99%) emerged as the sole vitamin-class compound. Remarkably, the triterpenoid cycloartenol dominated the profile at 40.27%, while α-amyrin and 24-methylenecycloartanol enriched terpenoid diversity. Additional constituents included hydroxyvalerenic acid and artemisinin B (1.53%), a sesquiterpene lactone, collectively forming a complex chemical matrix (Supplementary Table S4).

FAAO contained 37 fatty acids, with saturated fatty acids dominated by palmitic acid (C16:0, 5.87%), stearic acid (C18:0, 3.49%), and behenic acid (C22:0, 0.749%). Oleic acid (C18:1n9c, 26.1%) prevailed among monounsaturated fatty acids, while linoleic acid (C18:2n6c, 53%) constituted the predominant polyunsaturated fatty acid, followed by α-linolenic acid (C18:3n3, 0.11%). Trace amounts of γ-linolenic acid (C18:3n6, ≤0.0026%), arachidic acid (C20:0, 0.259%), and lignoceric acid (C24:0, 0.259%) were also detected (Supplementary Table S5).

3.2. SSO and FAAO Protect HaCaT Cells from UVB Damage by Enhancing Cell Viability and Inhibiting Inflammation

To investigate the effects of SSO and FAAO on UVB-irradiated HaCaT cells, we first evaluated their cytotoxicity (Figure 1A). First, DMSO exhibited no significant toxicity to HaCaT cells at concentrations ≤ 1%. Cytotoxicity becomes greater as the concentration of DMSO increases (Figure 1B); therefore, we chose 1% DMSO as the solvent for SSO and FAAO. The results showed that the maximum safe concentration of FAAO was 0.1%, while SSO was not significantly cytotoxic even at 1% (Figure 1C,D).

Given the known cytotoxic effects of UVB radiation, we subsequently evaluated the protective efficacy of both oils on HaCaT keratinocytes following UVB exposure. To establish appropriate experimental parameters, we first conducted UVB dose–response studies to determine the median lethal dose (LD_{50}) for HaCaT cells. Through quantitative crystal violet staining, a well-established method for assessing adherent cell viability, we identified 500 J/m^2 as the UVB dose resulting in 50% cell mortality (LD_{50}) (Figure 1E). This standardized dose was subsequently employed in all photoprotection cell-based assays. Subsequently, we evaluated the photoprotective efficacy of various concentrations of SSO and FAAO (all below the predetermined safety threshold) on HaCaT cells exposed to 500 J/m^2 UVB radiation. Quantitative analysis revealed that 0.25% SSO and 0.1% FAAO demonstrated optimal protection ability against UVB-induced cell mortality (Figure 1F,G). Given that UVB irradiation triggers inflammatory responses, we investigated the anti-inflammatory properties of SSO and FAAO by quantifying *IL-6*, *IL-1β*, and *TNF-α* expression in HaCaT cells. The result revealed that UVB exposure significantly elevated *IL-6* and *TNF-α* expression (Figure 1H–J), while both oils significantly suppressed UVB-induced *IL-6* production (Figure 1I). Neither affected *IL-1β* levels (Figure 1H). Notably, only FAAO demonstrated significant inhibition of *TNF-α* expression (Figure 1J). These findings indicate that SSO and FAAO mitigate UVB-induced cellular damage through enhancing cell viability and selectively modulating pro-inflammatory cytokine production. This synergistic action underscores their potential as natural photoprotective and anti-inflammatory agents for dermatological applications.

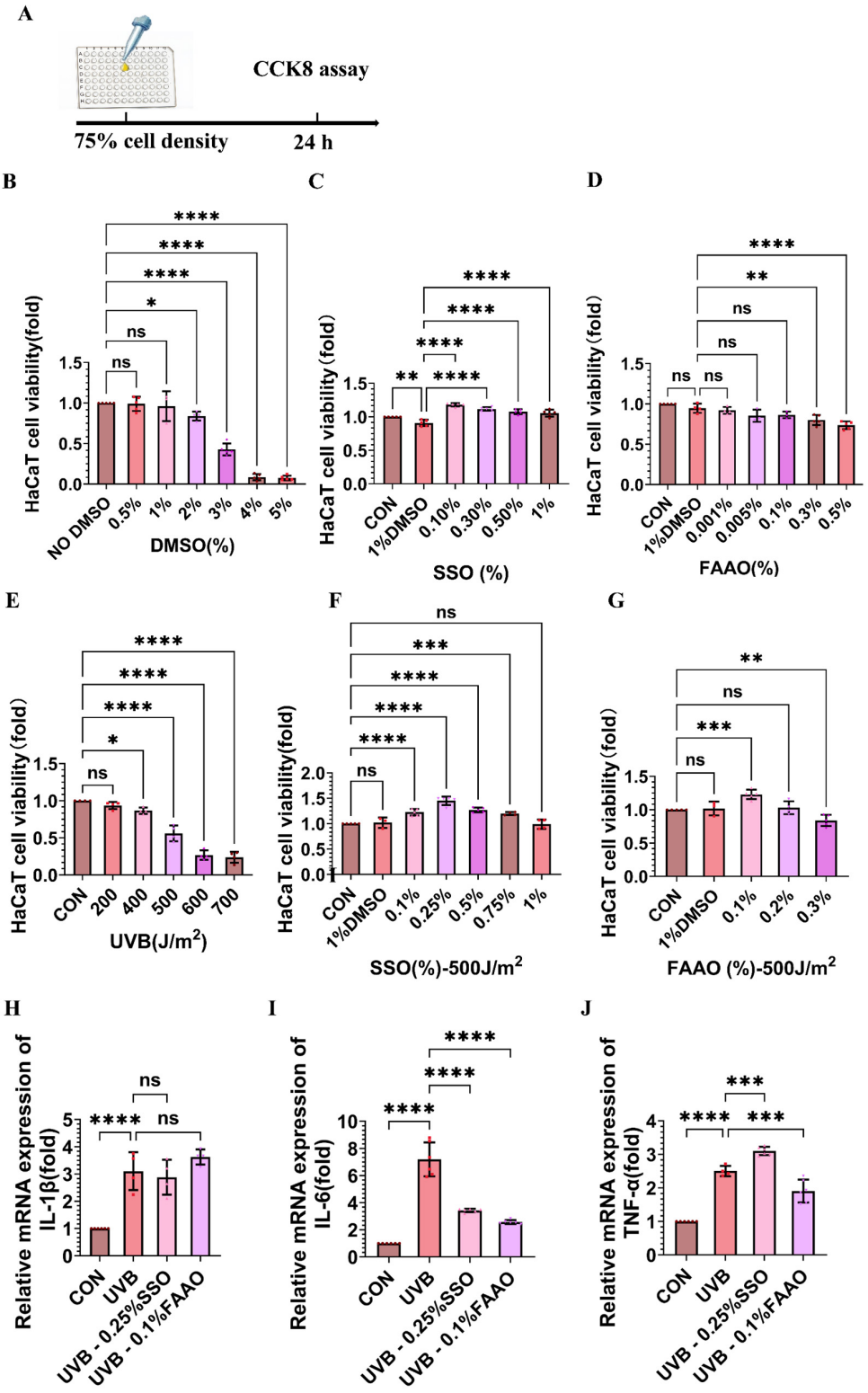

Figure 1. SSO and FAAO protect HaCaT cells from UVB damage by enhancing cell viability and inhibiting inflammation. (**A**) Diagram of the experimental design used to determine the maximum safe concentration of DMSO and both oils, and the characterization of UVB. Maximum safe concentration assay of HaCaT cells on DMSO (**B**), SSO (**C**), and FAAO (**D**). (**E**) LD_{50} of UVB on HaCaT cells. The effect of SSO (**F**) and FAAO (**G**) on UVB-treated HaCaT cells. (**H**–**J**) Quantitative RT-PCR to detect the effects of SSO and FAAO on *IL-1β*, *IL-6* and *TNF-α* expression in UVB-treated HaCaT cells. Data are presented as mean ± standard error of the mean (n ≥ 3). Not significant (ns) = $p > 0.05$, * $p < 0.05$, ** $p < 0.01$, *** $p < 0.001$, **** $p < 0.0001$.

3.3. Establishment of a UVB-Induced Skin Barrier Injury Mouse Model

In order to verify the protective effects of SSO and FAAO against UVB in vivo, the skin barrier damage mouse model was constructed by irradiating SKH-1 mice with UVB four times every other day (2000 J/m^2 each time, minimum erythemal dose), with the dorsal skin tissues being collected on day 7 (Figure 2A). Serial photographic documentation obtained every 48 h revealed no visible cutaneous alterations immediately following initial UVB exposure (P1). However, characteristic scaly lesions became apparent after the second irradiation (P3), progressing to marked erythema, edema, and widespread desquamation by day 7 (Figure 2B). Quantitative TEWL measurements demonstrated: (1) baseline epidermal barrier function at P0 (pre-exposure); (2) a statistically significant increase in water loss beginning at P3; (3) maximal barrier disruption at P5; and (4) sustained dysfunction through day 7, confirming progressive and persistent impairment of stratum corneum integrity (Figure 2C). Histopathological assessment revealed significant epidermal hyperplasia following initial UVB exposure (P1), with thickness measurements peaking by P5 and maintaining significant elevation compared to non-irradiated controls (Figure 2D,E). This comprehensive dataset validates the successful development of a temporally progressive skin barrier injury model, characterized by progressive epidermal hyperproliferation and histopathological alterations, collectively establishing a robust platform for therapeutic intervention studies.

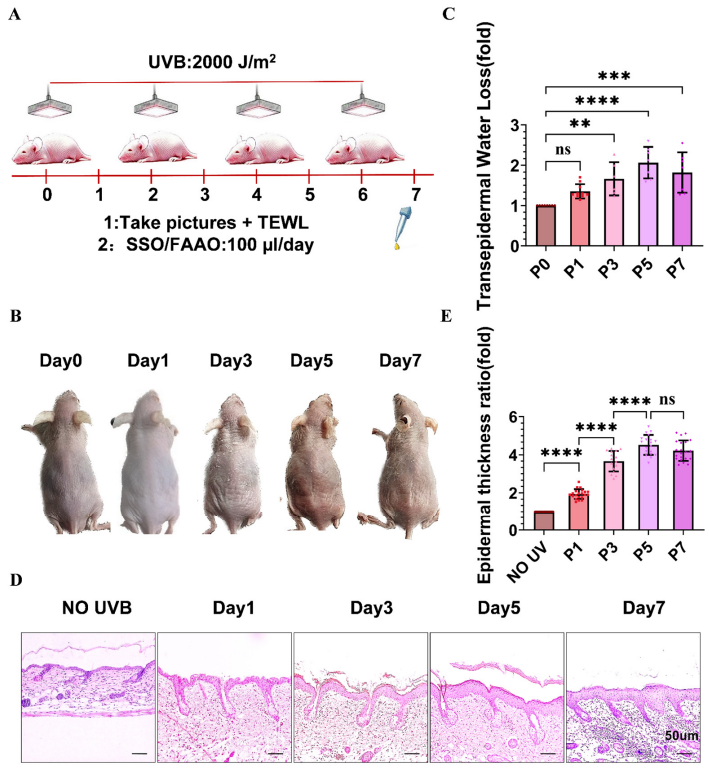

Figure 2. Establishment of a UVB-induced skin barrier injury model. (**A**) UVB irradiation protocol. (**B**) Temporal alterations in skin TEWL after UVB exposure. (**C**) TEWL changes at different times after UVB irradiation. (**D**,**E**) HE staining of dorsal skin and its statistical graph. Data are presented as mean ± standard error of the mean (n ≥ 3). Not significant (ns) = $p > 0.05$, ** $p < 0.01$, *** $p < 0.001$, **** $p < 0.0001$.

3.4. Synergistic Restoration of UVB-Induced Skin Barrier Dysfunction by a 1:1 SSO/FAAO Combination

To assess the reparative effects of SSO, FAAO, and their 1:1 combination (SSO/FAAO) on UVB-induced cutaneous damage, the oils were applied topically to murine dorsal skin 30 min before daily UVB exposure. Following seven days of repeated UVB irradi-

ation, progressive dermatological changes were observed, including erythema, edema, and desquamation (Figure 3A). Notably, no significant phenotypic improvements were observed in any treatment group during the initial three days of UVB exposure. By day 5, only the SSO/FAAO group exhibited discernible protective effects, whereas all three treatment groups showed partial attenuation of erythema by day 7. The SSO/FAAO group, however, displayed superior therapeutic efficacy, with markedly reduced edema and desquamation while maintaining consistent barrier protection throughout the experimental period (Figure 3A). Dynamic TEWL measurements revealed persistent barrier dysfunction across all groups, with no significant improvement in TEWL values despite topical treatment (Figure 3B). The persistent TEWL elevation despite histological recovery implies distinct repair mechanisms or differential temporal dynamics in barrier restoration.

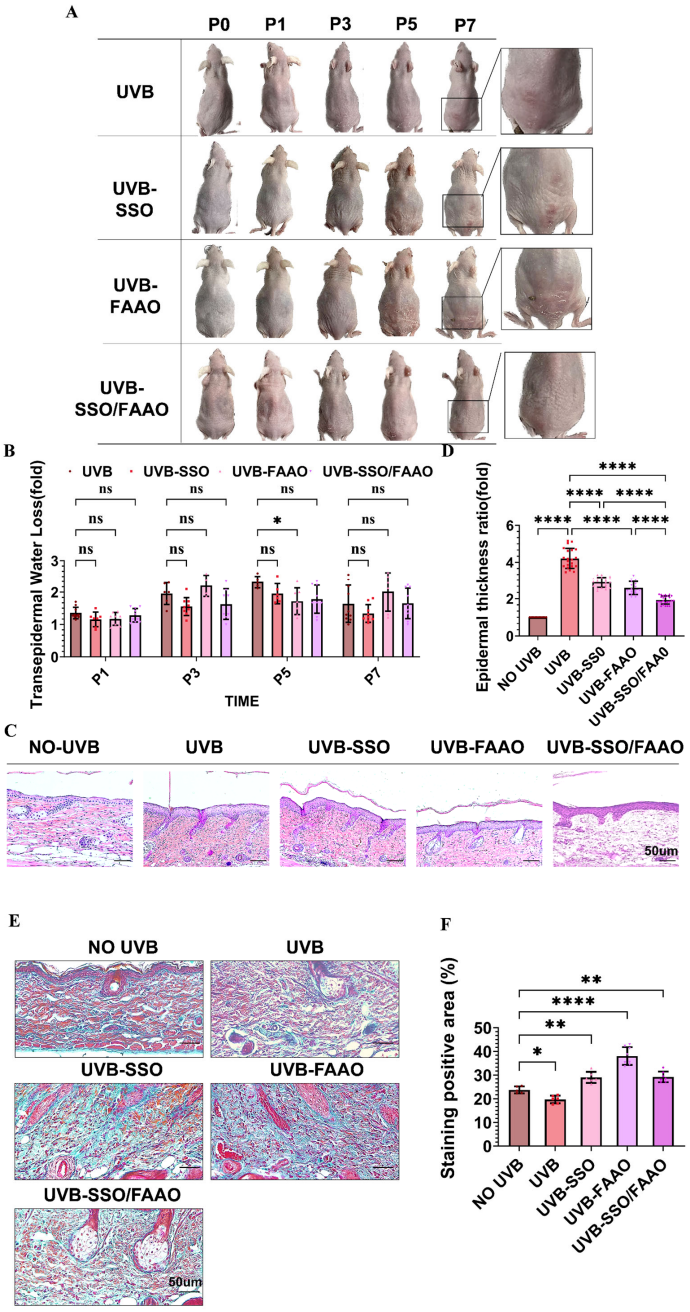

Figure 3. Synergistic restoration of UVB-induced skin barrier dysfunction by a 1:1 SSO-FAAO combination. (**A**) Representative photographs showing phenotypic progression in UVB-exposed mice following topical application of SSO, FAAO, and their combination at various time points. (**B**) Quantitative analysis

of TEWL measurements over time after treatment with SSO, FAAO, and their combination (no statistically significant differences were observed among groups). (**C**,**D**) HE staining demonstrating epidermal thickness changes in treated mice and their statistical analysis. (**E**,**F**) Masson staining showing changes in skin collagen in treated mice and statistical analysis. Data are presented as mean ± standard error of the mean (n ≥ 3). Not significant (ns) = $p > 0.05$, * $p < 0.05$, ** $p < 0.01$, **** $p < 0.0001$.

Histopathological analysis revealed that UVB irradiation induced pronounced epidermal hyperplasia. While treatment with either SSO or FAAO alone attenuated this hyperproliferative response, SSO/FAAO exhibited the most pronounced effect, reducing epidermal thickness by approximately 50% compared to UVB-exposed control (Figure 3C,D). This histological improvement correlated with the observed macroscopic reduction in inflammatory phenotypes, further supporting the synergistic benefit of combining SSO and FAAO for epidermal architecture restoration. Additionally, Masson staining demonstrated significantly diminished collagen deposition in UVB-irradiated skin, a deficit that was effectively reversed by all three treatments (Figure 3E,F).

The above evidence suggests that although SSO and FAAO alone can partially improve UVB-induced barrier damage, their 1:1 formulation may significantly enhance the repair efficacy on the structural integrity of the epidermis and the barrier function through the synergistic effect between the components. As a result, the subsequent mechanism study will focus on the analysis of the action target of the formulation.

3.5. Molecular Mechanisms Underlying the SSO-FAAO Compound's Dual-Pathway Repair of UVB-Induced Damage

To investigate the molecular-level alterations induced by FAAO and SSO in UVB-damaged skin, we performed transcriptome sequencing on day 7 skin tissue samples from three experimental groups: (1) untreated control (CON), (2) UVB-exposed (UVB), and (3) UVB-exposed and treated with SSO-FAAO complex (UVB_Compound). Principal component analysis (PCA) revealed significant transcriptomic divergence between the CON and UVB groups. Notably, the UVB_Compound group exhibited a gene expression profile that shifted toward the CON group, indicating partial reversal of UVB-induced transcriptional dysregulation (Figure 4A). Comparative analysis identified 1743 differentially expressed genes (DEGs) between UVB and CON groups, and 4086 DEGs between UVB_Compound and UVB groups, with 1240 overlapping DEGs (Figure 4B,C). KEGG pathway enrichment analysis of these shared 1240 DEGs revealed significant enrichment in ECM-receptor interactions, VEGF signaling pathways, and lipid metabolism-related pathways (Figure 4D). The anti-inflammatory properties of the SSO-FAAO complex were further corroborated by heatmap analysis of key pathways, including VEGF and protein degradation/uptake pathways. Treatment significantly downregulated the expression of proinflammatory mediators, such as VEGFa, IL-17rc, S100a9, IL23a and RORC (Figure 4E). Consistent with these findings, qRT-PCR analysis revealed substantial reductions in pro-inflammatory cytokine levels (*IL-6*, *IL-1β*, and *TNF-α*) in treated tissues on day 7 (Figure 4F–H). Moreover, the compound treatment effectively reversed UVB-mediated suppression of collagen (COL1A2, COL4A1, COL5A1, COL17A1) and laminin (LAMA2, LAMB1, LAMB2, LAMC1) gene expression (Figure 4I), thereby promoting extracellular matrix remodeling.

Naturally, 7-day UVB irradiation triggered a systemic immune response, marked by increased $CD45^+$ leukocyte infiltration, which was significantly suppressed by both FAAO and SSO/FAAO (Figure 5A). Further analysis revealed that UVB exposure also induced innate immune activation, as evidenced by enhanced $F4/80^+$ macrophage recruitment (Figure 5B), indicating the establishment of a localized inflammatory microenvironment. Notably, topical application of SSO, FAAO, and SSO/FAAO effectively suppressed macrophage recruitment, with the SSO/FAAO group exhibiting the most pronounced in-

hibitory effect (Figure 5B). This indicates that UVB radiation triggers the activation of skin innate immunity, while the combined application of SSO and FAAO effectively suppresses the inflammatory response, which aligns with the aforementioned RNA sequencing results.

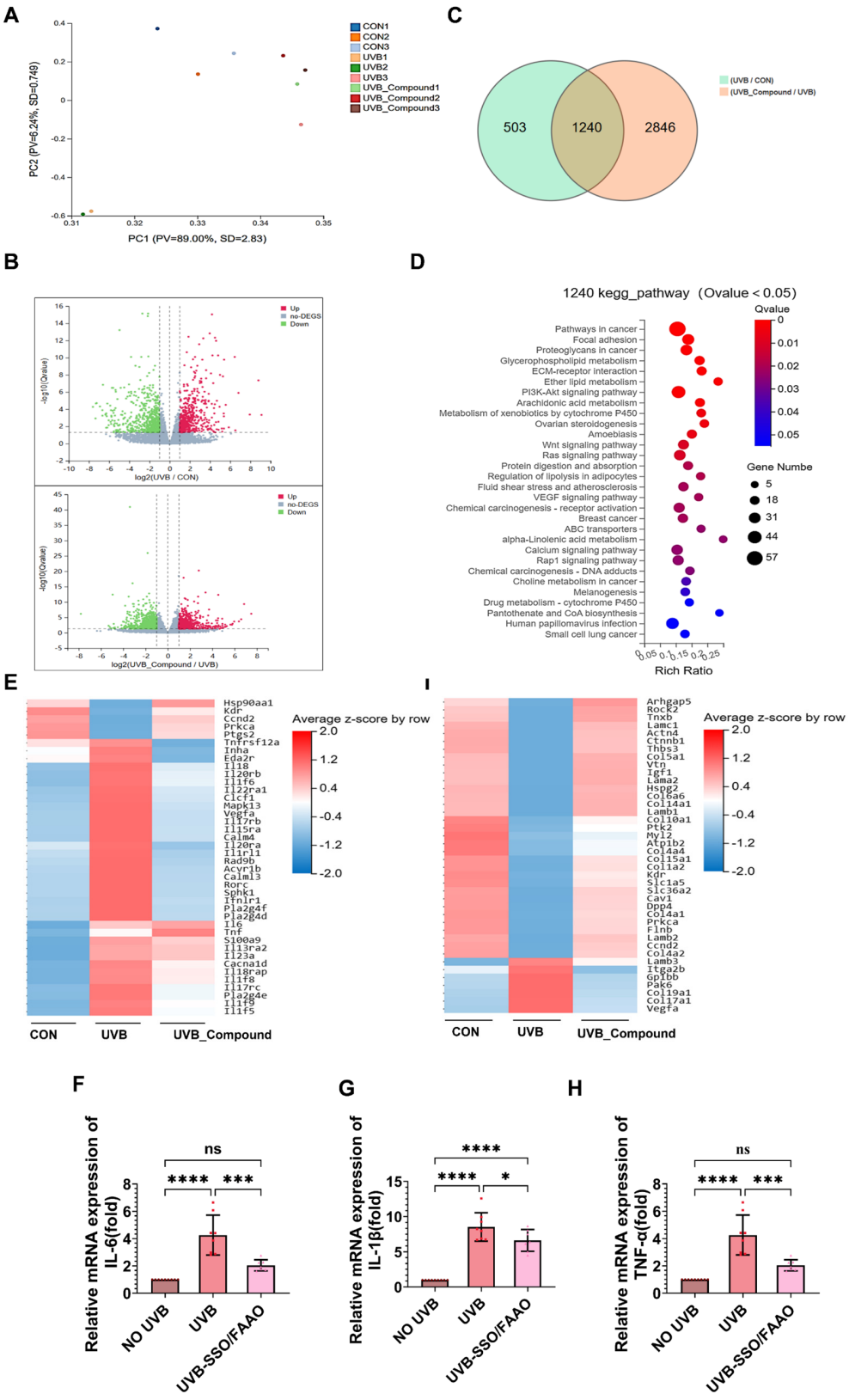

Figure 4. Transcriptomic sequencing of skin tissues treated with oils. (**A**) Principal component analysis for CON, UVB, and UVB_Compound. (**B**) Differential gene scatter plots for UVB/CON (top) and UVB_Compound/UVB (bottom) (up-regulation: Log2fc > 1, down-regulation: Log2fc < −1. Vertical

dashed lines indicate $\log_2$(fold change) = ±1, and the horizontal dashed line represents the threshold of Q-value ≤ 0.05). (**C**) VENN/UpSetR plots of differential gene sets in UVB/CON and UVB_Compound/UVB. (**D**) KEGG-enrichment analysis at the intersection (1240) of the differential gene set of UVB/CON and UVB_Compound/UVB. (**E**) Heatmaps of selected inflammatory pathway-related genes (q < 0.05) in CON, UVB, and UVB_Compound based on the shared 1240 DEGs. (**F**–**H**) *TNFα*, *IL-6*, and *IL-1β* expression detected by RT-PCR. (**I**) Heatmaps of selected genes related to ECM receptor interaction and protein digestion and uptake pathways (q < 0.05) based on the shared 1240 DEGs. Data are presented as mean ± standard error of the mean (n ≥ 3). Not significant (ns) = $p > 0.05$, * $p < 0.05$, *** $p < 0.001$, **** $p < 0.0001$.

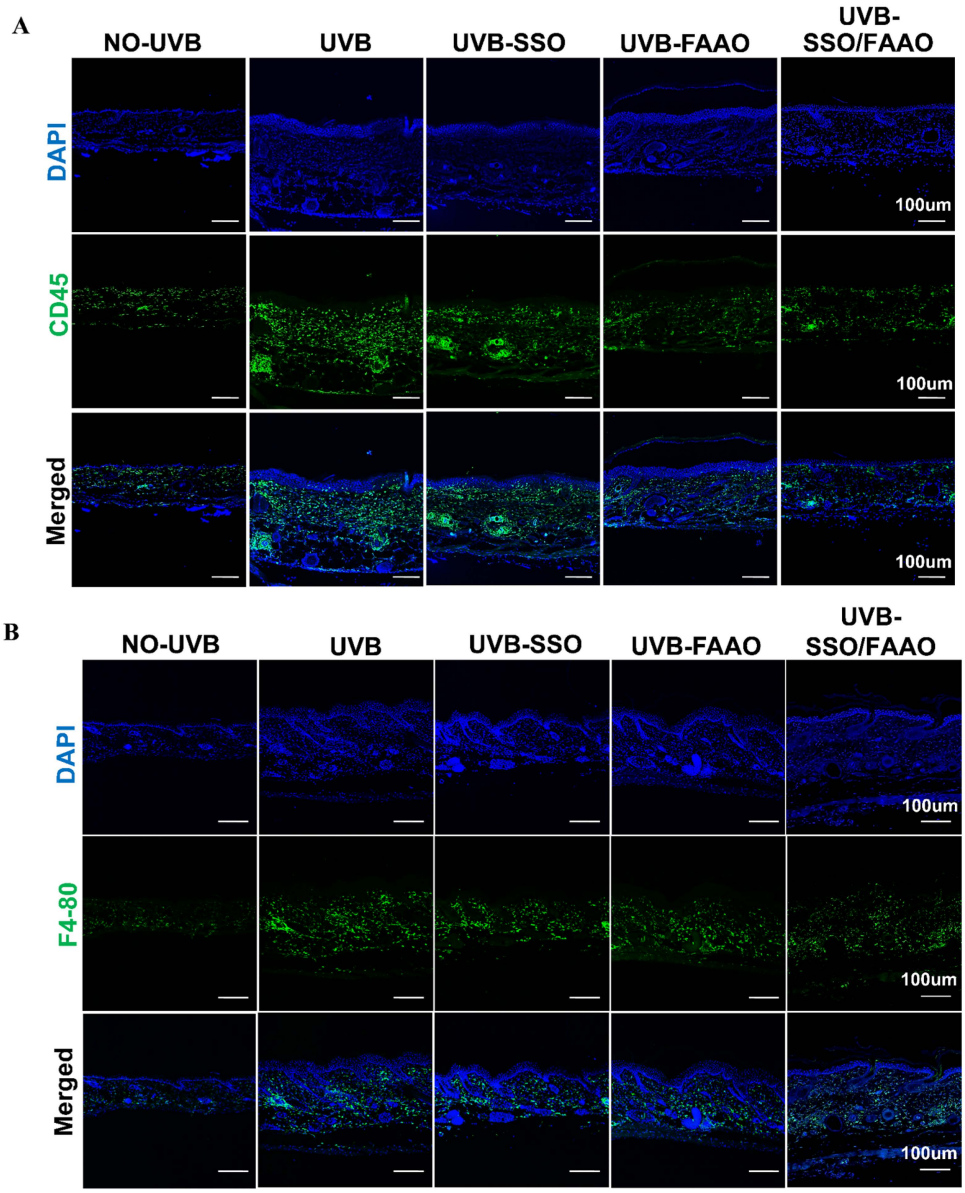

Figure 5. Representative immunofluorescence images showing CD45 leukocyte infiltration (**A**) and F4/80$^+$ macrophage infiltration (**B**) in UVB-damaged skin on day 7 post-treatment with SSO and FAAO.

Collectively, these findings suggest that the SSO/FAAO combination repairs UVB-induced photodamage by suppressing immune cell recruitment and inflammatory factor expression, while promoting extracellular matrix remodeling in the skin.

4. Discussion

This study provides a comprehensive mechanistic investigation into the reparative effects exerted by plant-derived oils (SSO, FAAO) and their combinatorial formulation against UVB-induced skin barrier impairment, employing an integrated experimental approach combining in vitro and in vivo models. In UVB-irradiated HaCaT cells, SSO (0.25%) and FAAO (0.1%) exhibited different anti-inflammatory efficacies. While both oils inhibited IL-6 expression, FAAO demonstrated unique potency in suppressing TNF-α expression, indicating pathway-specific modulation of inflammatory responses.

In the SKH-1 hairless mice, UVB-induced barrier disruption manifested as elevated TEWL, epidermal hyperplasia, and immune cell infiltration ($F4/80^+$ macrophages, $CD45^+$ leukocytes). Although individual treatment with either SSO or FAAO partially restored normal epidermal thickness, the 1:1 SSO/FAAO combination exhibited superior therapeutic efficacy, simultaneously improving both macroscopic inflammation (erythema, edema) and microscopic epidermal reorganization. Notably, only the combined formulation significantly reduced both leukocyte and macrophage infiltration. These findings highlight the distinct advantage of multi-target therapeutic strategies for comprehensive photodamage repair. Transcriptomic analysis revealed the polypharmacological mechanism underlying the SSO-FAAO combination's therapeutic effects. The dual "anti-inflammatory–reparative" mode simultaneously suppressed UVB-activated VEGF signaling (inhibiting both angiogenesis and inflammatory cascades), and enhanced ECM-receptor interactions (promoting collagen synthesis and ECM remodeling). Notably, while immediate barrier function recovery (as measured by TEWL) showed limited improvement, the formulation promoted fundamental tissue restoration through two key mechanisms: ECM homeostasis reestablishment and immune microenvironment normalization. These findings suggest a sequential paradigm in skin barrier repair, where structural reconstitution precedes functional recovery.

GC-MS analysis revealed a predominance of polyunsaturated fatty acids (PUFAs) in SSO, which are critical for skin barrier integrity. Clinical studies demonstrated that n-3 PUFAs alleviate psoriasis by suppressing inflammatory cytokines [19], while in vitro models show α-linolenic and linoleic acids enhance barrier function through incorporation into phospholipids/triglycerides and regulation of bioactive lipids [20]. Notably, betulin in SSO exhibits anti-inflammatory activity via NF-κB/MAPK pathway inhibition and NLRP3 inflammasome suppression [21], highlighting its therapeutic relevance for inflammatory skin conditions. Furthermore, the intricate chemical profile underpins FAAO's potential dermatological efficacy. Experimental evidence indicates β-caryophyllene reduces expression of Toll-like receptor-4, IL-6, and TNF-α in diet-induced obese mice [22]. Artemisinin B dose-dependently suppresses TNF-α-induced NF-κB reporter gene expression in TPA-stimulated murine skin inflammation models [23]. Key components including oleic acid [24], linoleic acid [24], squalene [25], and sterols [26] exhibit anti-inflammatory and antioxidant properties. Although vitamin E occurs at low concentrations (0.02–0.04%), its radical-scavenging capacity inhibits lipid peroxidation cascades, indirectly preserving epidermal barrier integrity [27].

While this study provides significant mechanistic insights, several limitations should be acknowledged: (1) Although we focused on IL-6 and TNF-α as canonical inflammatory mediators, other cytokine networks and signaling pathways may participate in the observed therapeutic effects; (2) the specific bioactive constituents responsible for the pharmacological effects of SSO and FAAO remain to be identified and characterized; and (3) the translational potential of these findings requires further validation using human skin models, as murine epidermal responses may not fully recapitulate human skin physiology.

5. Conclusions

In summary, this study demonstrates that the therapeutic potential of SSO and FAAO, which contain linoleic acid and artemisinin derivatives, respectively, promotes post-UVB barrier repair. Using a murine UVB model, we observed that the 1:1 SSO/FAAO formulation significantly enhances the repair efficacy on the structural integrity of the epidermis and the barrier function through the synergistic effect between the components. Mechanistically, SSO/FAAO formulation promotes epidermal barrier recovery by attenuating inflammatory responses and promoting extracellular matrix remodeling. These findings not only validate existing reports on lipid-mediated regulation of inflammatory cascades, but also highlight the necessity of personalized application of botanical extracts based on specific inflammatory disease profiles in clinical practice.

Supplementary Materials: The following supporting information can be downloaded at: https://www.mdpi.com/article/10.3390/cosmetics13020077/s1, Figure S1: GC-MS Total Ion Chromatogram of SSO.; Figure S2: GC-MS Total Ion Chromatogram of FAAO; Table S1: Primer list used for RT-PCR; Table S2: Relative Mass Content of SSO Components; Table S3: Fatty Acid Composition Analysis of SSO (High-Mass Fraction); Table S4: Relative Mass Content of FAAO Components; Table S5: Fatty Acid Composition Analysis of SSO (High-Mass Fraction).

Author Contributions: J.L.: Investigation, Validation, Methodology, Formal analysis, Writing—original draft. Q.W.: Investigation, Validation, Methodology, Formal analysis. J.Z.: Investigation, Validation. X.W.: Resources, Methodology. M.Z.: Resources, Methodology. Y.W.: Validation, Data curation. Y.Z.: Resources, Methodology. L.Z.: Resources, Methodology. R.L.: Resources, Methodology, Formal analysis. H.J.: Resources, Methodology, Formal analysis. G.M.: Writing—review and editing, Supervision, Project administration, Funding acquisition, Conceptualization. All authors have read and agreed to the published version of the manuscript.

Funding: This research was funded by the National Nature Science Foundation of China (No. 32570986) and the Natural Science Foundation of Shanghai (No. 23ZR1431900).

Institutional Review Board Statement: The study was conducted in accordance with the Declaration of Helsinki, and approved by the Ethics Committee of Shanghai Jiao Tong University (B20250136P, 26 February 2025). The animal study protocol was approved by the Ethics Committee of Shanghai Jiao Tong University (202501124, 24 February 2025).

Informed Consent Statement: Not applicable.

Data Availability Statement: The data presented in this study are available on request from the corresponding author.

Conflicts of Interest: Q.W., Y.Z., L.Z., R.L. and H.J. are employed by Shanghai Jahwa United Co., Ltd. The company had no role in the design of the study; in the collection, analyses or interpretation of data; in the writing of the manuscript; or in the decision to publish the results.

Abbreviations

The following abbreviations are used in this manuscript:

SSO	Safflower seed oil
FAAO	Fermented *Artemisia annua* oil
UVB	Ultraviolet radiation
MED	Minimal erythema dose
TEWL	Transepidermal water loss
GC-MS	Gas Chromatography-Mass Spectrometry
KEGG	Kyoto Encyclopedia of Genes and Genomes

References

1. Belokhvostova, D.; Berzanskyte, I.; Cujba, A.M.; Jowett, G.; Marshall, L.; Prueller, J.; Watt, F.M. Homeostasis, regeneration and tumour formation in the mammalian epidermis. *Int. J. Dev. Biol.* **2018**, *62*, 571–582. [CrossRef]
2. Harry, J. Anatomy and physiology of the skin. *Br. J. Nurs.* **2025**, *4*, 754–760. [CrossRef]
3. De Szalay, S.; Wertz, P.W. Protective Barriers Provided by the Epidermis. *Int. J. Mol. Sci.* **2023**, *24*, 3145. [CrossRef]
4. Gardeazabal, L.; Izeta, A. Elastin and collagen fibres in cutaneous wound healing. *Exp. Dermatol.* **2024**, *33*, e15052. [CrossRef]
5. Nestle, F.O.; Di Meglio, P.; Qin, J.Z.; Nickoloff, B.J. Skin immune sentinels in health and disease. *Nat. Rev. Immunol.* **2009**, *9*, 679–691. [CrossRef]
6. Gollogly, J.M.; Nguyen, J.K.; Lau, D.; Austin, E.; Jagdeo, J. Updates on the Molecular Basis of Photoaging in All Skin Types. *J. Drugs Dermatol.* **2024**, *23*, 504–509. [PubMed]
7. Xia, J.; Song, X.; Bi, Z.; Chu, W.; Wan, Y. UV-induced NF-kappaB activation and expression of IL-6 is attenuated by (-)-epigallocatechin-3-gallate in cultured human keratinocytes in vitro. *Int. J. Mol. Med.* **2005**, *16*, 943–950. [PubMed]
8. Ansary, T.M.; Hossain, M.R.; Kamiya, K.; Komine, M.; Ohtsuki, M. Inflammatory Molecules Associated with Ultraviolet Radiation-Mediated Skin Aging. *Int. J. Mol. Sci.* **2021**, *22*, 3974. [CrossRef]
9. Skobowiat, C.; Sayre, R.M.; Dowdy, J.C.; Slominski, A. Ultraviolet radiation regulates cortisol activity in a waveband-dependent manner in human skin ex vivo. *Br. J. Dermatol.* **2013**, *168*, 595–601. [CrossRef] [PubMed]
10. Kaltchenko, M.V.; Chien, A.L. Photoaging: Current Concepts on Molecular Mechanisms, Prevention, and Treatment. *Am. J. Clin. Dermatol.* **2025**, *26*, 321–344. [CrossRef]
11. Banno, T.; Gazel, A.; Blumenberg, M. Effects of tumor necrosis factor-alpha (TNF alpha) in epidermal keratinocytes revealed using global transcriptional profiling. *J. Biol. Chem.* **2004**, *279*, 32633–32642. [CrossRef] [PubMed]
12. Ciążyńska, M.; Olejniczak-Staruch, I.; Sobolewska-Sztychny, D.; Narbutt, J.; Skibińska, M.; Lesiak, A. Ultraviolet Radiation and Chronic Inflammation—Molecules and Mechanisms Involved in Skin Carcinogenesis: A Narrative Review. *Life* **2021**, *11*, 326. [CrossRef] [PubMed]
13. Nakajima, K.; Kataoka, S.; Sato, K.; Takaishi, M.; Yamamoto, M.; Nakajima, H.; Sano, S. Stat3 activation in epidermal keratinocytes induces Langerhans cell activation to form an essential circuit for psoriasis via IL-23 production. *J. Dermatol. Sci.* **2019**, *93*, 82–91. [CrossRef]
14. Feldmeyer, L.; Keller, M.; Niklaus, G.; Hohl, D.; Werner, S.; Beer, H.-D. The inflammasome mediates UVB-induced activation and secretion of interleukin-1beta by keratinocytes. *Curr. Biol. CB* **2007**, *17*, 1140–1145. [CrossRef] [PubMed]
15. Elbediwy, A.; Thompson, B.J. Evolution of mechanotransduction via YAP/TAZ in animal epithelia. *Curr. Opin. Cell Biol.* **2018**, *51*, 117–123. [CrossRef]
16. Kapoor, R.; Huang, Y.S. Gamma linolenic acid: An antiinflammatory omega-6 fatty acid. *Curr. Pharm. Biotechnol.* **2006**, *7*, 531–534. [CrossRef]
17. Gęgotek, A.; Jastrząb, A.; Jarocka-Karpowicz, I.; Muszyńska, M.; Skrzydlewska, E. The Effect of Sea Buckthorn (*Hippophae rhamnoides* L.) Seed Oil on UV-Induced Changes in Lipid Metabolism of Human Skin Cells. *Antioxidants* **2018**, *7*, 110. [CrossRef]
18. Lehmann, B. HaCaT Cell Line as a Model System for Vitamin D3 Metabolism in Human Skin. *J. Investig. Dermatol.* **1997**, *108*, 78–82. [CrossRef]
19. Morin, S.; Simard, M.; Rioux, G.; Julien, P.; Pouliot, R. Alpha-Linolenic Acid Modulates T Cell Incorporation in a 3D Tissue-Engineered Psoriatic Skin Model. *Cells* **2022**, *11*, 1513. [CrossRef]
20. Simard, M.; Tremblay, A.; Morin, S.; Martin, C.; Julien, P.; Fradette, J.; Flamand, N.; Pouliot, R. α-Linolenic acid and linoleic acid modulate the lipidome and the skin barrier of a tissue-engineered skin model. *Acta Biomater.* **2022**, *140*, 261–274. [CrossRef]
21. Szlasa, W.; Ślusarczyk, S.; Nawrot-Hadzik, I.; Abel, R.; Zalesińska, A.; Szewczyk, A.; Sauer, N.; Preissner, R.; Saczko, J.; Drag, M.; et al. Betulin and Its Derivatives Reduce Inflammation and COX-2 Activity in Macrophages. *Inflammation* **2023**, *46*, 573–583. [CrossRef]
22. Franco-Arroyo, N.N.; Viveros-Paredes, J.M.; Zepeda-Morales, A.S.M.; Roldan, E.; Marquez-Aguirre, A.L.; Zepeda-Nuno, J.S.; Velazquez-Juarez, G.; Fafutis-Morris, M.; Lopez-Roa, R. β-Caryophyllene, a Dietary Cannabinoid, Protects Against Metabolic and Immune Dysregulation in a Diet-Induced Obesity Mouse Model. *J. Med. Food* **2022**, *25*, 993–1002.
23. Wang, K.S.; Li, J.; Wang, Z.; Mi, C.; Ma, J.; Piao, L.X.; Xu, G.H.; Li, X.; Jin, X. Artemisinin inhibits inflammatory response via regulating NF-κB and MAPK signaling pathways. *Immunopharmacol. Immunotoxicol.* **2017**, *39*, 28–36. [CrossRef] [PubMed]
24. Cardoso, C.R.; Favoreto, S.; Oliveira, L.L.; Vancim, J.O.; Barban, G.B.; Ferraz, D.B.; Silva, J.S. Oleic acid modulation of the immune response in wound healing: A new approach for skin repair. *Immunobiology* **2011**, *216*, 409–415. [CrossRef] [PubMed]
25. Cárdeno, A.; Aparicio-Soto, M.; Montserrat-de la Paz, S.; Bermudez, B.; Muriana, F.J.; Alarcón-De-La-Lastra, C. Squalene targets pro- and anti-inflammatory mediators and pathways to modulate over-activation of neutrophils, monocytes and macrophages. *J. Funct. Foods* **2015**, *14*, 779–790. [CrossRef]

26. Kopylov, A.T.; Malsagova, K.A.; Stepanov, A.A.; Kaysheva, A.L. Diversity of Plant Sterols Metabolism: The Impact on Human Health, Sport, and Accumulation of Contaminating Sterols. *Nutrients* **2021**, *13*, 1623. [CrossRef]
27. Heo, J.I.; Kim, M.J.; Kim, D.; Seo, J.; Moon, J.H.; Choi, S.H.; Lee, H.J.; Oh, T.J. Alpha-Tocopherol-Loaded Liposomes Reduce High Glucose Induced Oxidative Stress in Schwann Cells: A Proof of Concept Study. *Diabetes Metab. J.* **2025**, *49*, 507–512. [CrossRef]